This paper appears in Control Engineering Practice, 2017
DOI: 10.1016/j.conengprac.2017.04.001
Vol. 63, June 2017, Pages 34-43

Sliding-based Image-guided 3D Needle Steering in Soft Tissue

Bita Fallahi[a,*], Carlos Rossa[a], Ron S. Sloboda[b], Nawaid Usmani[b], Mahdi Tavakoli[a]

[a] *Department of Electrical and Computer Engineering, University of Alberta, Edmonton, AB, Canada, T6G 1H9*
[b] *Cross Cancer Institute and the Department of Oncology, University of Alberta, Edmonton, AB, Canada, T6G 1Z2*

Abstract

This paper presents a sliding-based method for steering beveled-tip needles in a 3D environment. The controller determines the needle roll angle using the needle tip position deviation, obtained from ultrasound images, and its first time derivative. The stability of the closed-loop system is analyzed using 3D unicycle model for the needle, as a result of which parameter constraints are derived. In this method the needle is steered by performing adjustments of needle orientation, which reduces the tissue trauma and injury. The performance of this method is verified by performing experiments using phantom tissue for environments with and without obstacles.

Keywords: medical robotics; needle steering; 3D environment; obstacle avoidance; sliding mode control

1. Introduction

1.1. Related Works

Robotic structures can be employed in needle insertion procedures such as brachytherapy, biopsy and neurosurgery to improve the needle targeting accuracy and efficiency of the procedure. In these procedures, long flexible beveled-tip needles are inserted into the human body for diagnosis, drug delivery or sample removal. Due to the needle/tissue interaction forces, the needle bends as it is inserted into the tissue and deflects from the desired path. This deflection makes the steering problem very challenging. Some of the issues in modeling and controlling beveled-tip needles are discussed in [1].

As the needle is inserted in tissue, it bends according to the bevel orientation. This dependency can be used to steer the needle to the target point and avoid an obstacle present on the needle's path. The bevel orientation changes by axially rotating the needle at its base, which is considered as the control input. By successively changing the bevel orientation at different depths, the needle moves in different directions in a 3D environment and deflects in different directions.

There have been different steering methods proposed in the literature that can be classified as planning algorithms and control algorithms. In motion planning methods, mathematical models are employed to determine the necessary actions at current and future times to reach the target as adjustments in the desired trajectory are performed to compensate for the modeling and implementation errors. In control algorithms, different control strategies are implemented as a feedback loop where the control actions are generated by the controller at the current time. Although control methods can also include path planning and/or re-planning to find feasible paths, the procedure for determining the system input is different.

In the literature, path planning methods have been developed both in 2D and 3D environments. In [2], a planner is presented to find the optimal path that brings the needle tip to a desired point in tissue. In [3] rotations are performed to move the needle on a straight line where the rotation depths are calculated from the force sensor and the flexible beam model for the needle. A planner for a needle in stiff tissue in a 3D environment with no obstacles is developed in [4]. To account for environments with obstacles, in [5], the potential field planning technique is used for steering the needle

*Corresponding author.
Email Address: fallahi@ualberta.ca (B. Fallahi)

tip and avoiding obstacles in 2D space. In [6] a planning algorithm is proposed in 2D space and [7, 8] present planners in 3D space. Extending the planar motion to 3D, in [9] a sequence of needle rotations are performed to compensate for the out of plane motions. A rapidly exploring random tree-based motion planner is employed in [10] and [11] to perform real-time re-plannings to steer the needle to the desired position. However, in these papers duty cycled spinning is employed to achieve different path curvatures. In [12], it is shown that by duty cycled spinning, the needle can move on paths with variable curvatures. Duty-cycled spinning has a drilling effect on tissue, which may cause tissue trauma.

From a control perspective, in [13], the controllability of the needle in soft tissue is studied using a dynamic model. In [14], using an ultrasound-based deflection predictor, a 2D semi-automated needle steering strategy is developed. In this approach the surgeon is in charge of needle insertion to ensure the safety of the operation, while the needle tip bevel location is robotically controlled to minimize the targeting error. The authors in [15] proposed a mechanics-based model of needle steering and developed a nonlinear model predictive controller (MPC) for 2D needle steering using iterative optimization of the predictions [16]. In [17], planning and control methods are combined where geometric and trigonometric relations between the needle's current position and the target are used in a feedback loop. In some of these algorithms, the exact knowledge of system parameters such as the needle's path curvature or its maximum value is needed. In [18], a sliding mode controller is presented which is based on the 3D unicycle model proposed in [19]. In this method a 5DOF magnetic tracking sensor is used which is combined with a with Kalman filter to provide the full information about the needle tip position and orientation. Measuring the orientation requires utilizing a sensor such as a needle-mounted electromagnetic tracking sensor, which itself suffers from sterilization and size issues. Since suitable sensors are not accessible, state observers can be employed to estimate the needle tip orientation using the measured needle tip position [20, 21]. Besides, if orientation observers or estimators are going to be used, the overall stability of the observer/controller loop should be studied, which is not a trivial task.

In brachytherapy procedures, the therapy is performed by implanting radioactive seeds at pre-planned locations in and around the tumor. The seeds are loaded within the hollow needle shaft and are deposited on the needle tip path as the needle is retracted. In this case, not only the needle tip position but also the needle track affects the procedure accuracy. According to pre-operative planning, it is desired to move the needle on a straight path (seed dosimetry planning). In our previous work [22], a sliding-mode controller in 2D space is developed, in which only a rough estimation of the needle path curvature suffices to ensure the stability of the system. In this method it is desired to reach a 2D point, which is specified by a desired deflection at a desired insertion depth. This is implemented by performneing 180° shaft rotations. Assuming the needle axial rotation to be much faster than the needle insertion velocity, the needle motion was considered to be planar. In practice, due to tissue inhomogeneity the needle makes out of plane motions, which is not accounted for in this method.

1.2. Contributions

In general, it is desired to develop strategies that provide control over the needle motion in 3D space and, in some special cases keep the needle moving on a straight line by making the deflection in different directions close to zero. This work extends our previous work [22] by steering the needle in 3D space as the needle is inserted to the desired depth and toward the desired position. This needle insertion system is driven with two inputs; the insertion velocity and needle axial rotational velocity. The depth can be controlled using the insertion velocity, by which the needle is pushed into the tissue. However, the needle deflection at each depth can be projected as the deflection in two different planes, which should be controlled using the other input, axial rotational velocity. From a feedback control perspective, the system suffers from under actuation: Using one control input, it is difficult to control two outputs (deflection in two directions). Besides, according to the kinematics of the system, the orientation of the needle tip, is highly involved in the system kinematics. However, it is not possible to measure the needle tip orientation using the ultrasound images due to the small diameter of the needle and the low resolution of the ultrasound images. The proposed method is based on the position measurements obtained from ultrasound images as no information about the needle tip orientation is used in the calculation of the control action. This is

beneficial as it removes the need for any orientation measurement or estimation tools.

The present work is a simple robust sliding-based control method, which is suitable for systems with parametric uncertainties and disturbances [23]. In the needle/tissue system, due to the tissue inhomogeneity, the needle/tissue interaction and the needle's path curvature encounter uncertainties, for which it is desired to design controllers robust with respect to uncertainties and disturbances. In the propose method the information from the ultrasound images is used, and no information about the needle or tissue properties is required to find the control signal. This work is a sliding-based method in which two surfaces are considered and the required rotation angle is found using these two sliding surfaces to compensate the tip deflection error in 3D space. The proposed method is then improved by using a adaptive-structure controller. In this scheme, the sliding surfaces are rotated. Such variable surfaces have been used in many different control applications for improving the performance [24, 25], smoothing the control[26], and reducing the chattering in image-guided applications [27]. This modification relaxes some constraints imposed by stability conditions. Moreover, it removes any dependence of the parameters on the needle path's curvature. The proposed method compensates for position errors by performing the required needle rotations, which can be very small adjustments to the needle orientation. This removes any unnecessary rotations and reduces the trauma on tissue caused by continuous rotations.

To verify the proposed method, experiments are performed for two different scenarios, i.e. 1-Moving the needle on a straight line and 2-moving the needle on a desired curved path to avoid an obstacle. In the second scenario, an offline planner is used to find a feasible path for the needle. However, the method does not depend on any specific planner and is general. Experimental results show a maximum targeting error of 1.14 mm, which is comparable to position errors obtained in the literature while reducing tissue trauma and risk of injury.

The paper is organized as follows. Section 2 presents the system equations. In section 3, the steering algorithm is introduced in which the fixed and adaptive structures are explained and the constraints for stability of the closed loop system are derived. Simulations and comparisons are provided in this section. Section 4 presents the planning algorithm used for finding a feasible path and the trajectory tracking problem. In section 5, the proposed method is validated for two different scenarios and the results are presented.

2. Background

As the needle is inserted into tissue, the trajectory traversed by the needle tip in 3D space is affected by the bevel orientation, which can be changed by axially rotating the needle base. Thus needle axial rotations can be used as a control input to change the bevel orientation and steer the needle to a desired position. The system equations can be written in the general form of

$$\dot{\mathbf{q}} = f(\mathbf{q}) + gu \tag{1}$$

in which, $\dot{()}$ represents the time derivative, u is the control input and $\mathbf{q} = \begin{bmatrix} x, & y, & z, & \alpha, & \beta, & \gamma \end{bmatrix}$ is the generalized coordinates which is well defined on

$$\mathcal{U} = \{\mathbf{q} \in \mathbb{R}^6 : \alpha, \gamma \in \mathbb{R}, \beta \in [-\pi/2, \pi/2]\} \tag{2}$$

and represent the position and orientation of the moving frame $\{B\}$ attached to the needle tip with respect to the fixed frame $\{A\}$ as shown in Fig.2.

(1) shows the kinematics of a beveled tip needle inserted into tissue, which can mathematically be expressed by the 3D unicycle equations using $Z-Y-X$ fixed angles as generalized coordinates with [20]

$$f = \begin{bmatrix} v\sin\beta \\ -v\cos\beta\sin\alpha \\ v\cos\alpha\cos\beta \\ kv\cos\gamma\sec\beta \\ kv\sin\gamma \\ -kv\cos\gamma\tan\beta \end{bmatrix} \tag{3a}$$

$$g = \begin{bmatrix} 0 & 0 & 0 & 0 & 0 & 1 \end{bmatrix}^T \tag{3b}$$

Here, k denotes the curvature of the needle path and v and is the needle insertion velocity. The position and orientation of frame $\{B\}$ are represented by vector $\begin{bmatrix} x & y & z \end{bmatrix}^T$ and the three angles α, β and γ, respectively. The orientation of the moving frame $\{B\}$ is found by three successive rotations of the moving frame around the fixed axes Z-Y-X by the values γ, β and α as shown in Fig.2

In (3), the needle insertion velocity v is used to insert the needle into the tissue, which is the primary motion of the needle toward the desired depth. As the needle moves in the insertion direction, the needle bends and the needle tip moves on

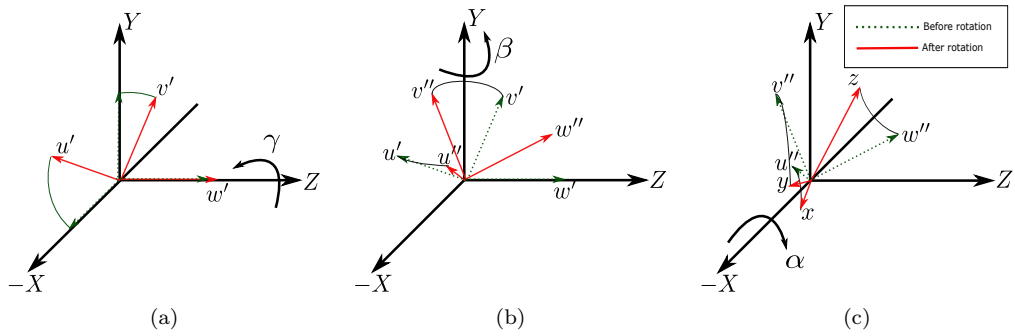

Figure 2: Successive rotations about the fixed axes. (a): roll angle γ about the Z axis. (b): pitch angle β about the Y axis. (c): yaw angle α about the X axis

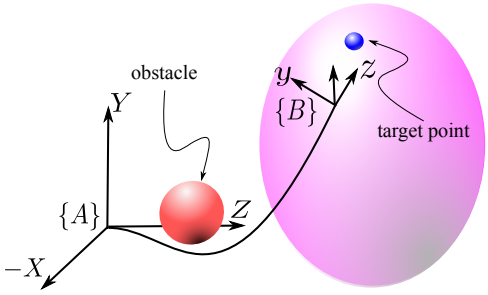

Figure 1: The needle in 3D space, target point and obstacle. Frame $\{A\}$ is the fixed frame and frame $\{B\}$ attached to the needle tip is the moving frame.

a curved path. In practical applications in which it is desired to involve the surgeon in the procedure, rather than automate the entire surgery (which raises safety concerns), the insertion can be performed by the surgeon while the axial rotations are calculated and implemented by a robotic system [28]. This provides the possibility of implementing semi-autonomous control in which the insertion is manually performed by the surgeon while the rotation is done robotically. In this work, in order to have an easy and repeatable framework for performing experiments, a fully-automated system is considered where the insertion is also performed by the robotic system. This can later be transferred to a semi-autonomous framework as the control algorithm is independent of the the insertion velocity. In this case the convergence and stability proof can be performed for the worst case of the lowest insertion velocity.

3. Steering method

The proposed method is based on determining the desired value of the needle roll angle γ that steers the needle to the desired deflection, which depends on the application. There are different applications for needle insertion systems such as biopsy and brachytherapy. In biopsy it is desired to reach a constant desired deflection, regardless of the path. In brachytherapy, the path traveled by the needle is important as the seeds are implanted on the needle track during the needle retraction. In this procedure the goal is to minimize the deflection at all depths, which is equivalent to have zero deflection at all times. In both cases the desired deflection values are constants. Having the desired value γ_d, the needle axial rotation velocity u can be found such that γ tracks the desired value γ_d, which steers the needle to the desired deflection. According to (3), having full control over γ requires knowledge of needle tip orientation, i.e., the angles γ and β. Measuring the orientation requires utilizing a needle-mounted sensor, which itself suffers from sterilization and size issues. Since suitable sensors are not accessible, state observers can be employed to estimate the needle tip orientation using the measured needle tip position [20, 21]. The estimation of the needle tip orientation is not a trivial task, which is not the focus of this work. In this paper the control strategy finds the desired value of the angle γ and is considered as the desired needle base angle. Since clinically used needles (also used in this paper) are torsionally highly stiff and also the curvature for these needles is very small, we have assumed that angle γ is equal to the needle base angle γ_d. Besides, since the method used here is based on sliding mode control, the method

will be robust with respect to these errors. The control structure is shown in Fig.3. In this figure, the control structure is implemented as a cascade loop. The inner loop uses a PID controller to control the needle base angle. The outer loop is a sliding mode control which determines the desired angle as the input of the inner loop. In other words, the sliding mode controller determines when and how much should the needle be rotated to have the error decreasing and the PID controller in the inner loop is responsible to rotate the needle to the desired angle, which is totally independent from the sliding mode controller proposed in the paper and is designed to be fast enough so its dynamics can be neglected.

3.1. Fixed structure

The main idea of a sliding mode controller is to define a suitable error dependent sliding surface S and the corresponding switching law to bring the system manifolds on the sliding surface and make it decreasing. To this end the switching law should make the time derivative of the Lyapunov function $V = \frac{1}{2}S^2$ negative definite, which is equivalent to a decreasing surface and consequently a decreasing error. Here, two sliding surfaces are defined for the x and y directions and the needle roll angle is switched in four different modes. Like all sliding based controllers, the system response consists of two phases, reaching phase and the sliding phase [23]. In reaching phase the system moves towards the desired surface $S_i = 0, (i = x, y)$ and in the sliding phase, in the ideal case, the system states remain on the desired surface, which makes the error go to zero. For the system considered here, the reaching phase is when the value of S_x and S_y are decreasing, however the sliding phase will never happen for this system as it does not have any equilibrium point other than the velocity being equal to zero. As long as the needle is being inserted, the velocities are changing and the needle bends. This will make the sliding phase involve chattering, which can be compensated for by accepting some bounds on error and performing the switches at some time intervals. This is equivalent to keep the sliding surfaces close to zero. To this end, define the following sliding surfaces

$$S_x = b_x \dot{e}_x + e_x \tag{4}$$

$$S_y = b_y \dot{e}_y + e_y \tag{5}$$

Having x_d and y_d as the desired deflection in the x and y directions, which should be reached at a certain depth, $e_x = x - x_d$ and $e_y = y - y_d$ represent the position error in the x and y directions, respectively, and b_x and b_y are the design parameters to be chosen later.

Considering the desired position in 3D space is a constant deflection at a certain depth, i.e. $\dot{x}_d = \dot{y}_d = 0$, the time derivative of the sliding surfaces equal:

$$\dot{S}_x = b_x \ddot{x} + \dot{x} \tag{6}$$

$$\dot{S}_y = b_y \ddot{y} + \dot{y} \tag{7}$$

Taking the time derivative of, $\dot{x}$ and $\dot{y}$ in (3) and substituting from (3), the above equations can be written as

$$\dot{S}_x = b_x k v^2 \cos\beta \sin\gamma + v \sin\beta \tag{8}$$

$$\dot{S}_y = -b_y k v^2 \cos\alpha \cos\gamma - b_y k v^2 \sin\beta \sin\alpha \sin\gamma + v \cos\beta \sin\alpha \tag{9}$$

In these equations, since $-\pi/2 \leq \beta \leq \pi/2$, it is assumed that $\cos\beta$ is always positive. As stated before, since in the sliding mode control the sign of the sliding surface and its derivative are of interest, considering the x direction, (8) consists of two terms on the right hand side, which can be positive or negative. If the absolute value of the first term is greater than the second term, regardless of the sign of the second term, $\dot{S}_x$ will have the same sign of the first term. Mathematically, this can be written as

$$|b_x k v^2 \cos\beta \sin\gamma| > v \sin\beta \tag{10}$$

if (10) is satisfied, using the assumption that $\cos\beta > 0, k > 0, b_x > 0$ and $v > 0$, then $\mathrm{sgn}(\dot{S}_x)$ is the same as the $\mathrm{sgn}(\sin\gamma)$. This inequality is equivalent to

$$|\sin\gamma| > \frac{1}{b_x k v} |\tan\beta| \tag{11}$$

Similarly for the y direction, if

$$|\cos\gamma| > |\sin\beta \tan\alpha \sin\gamma| + \frac{1}{b_y k v} |\cos\beta \tan\alpha| \tag{12}$$

$\mathrm{sgn}(\dot{S}_y)$ is determined by $-\mathrm{sgn}(\cos\gamma)$. Assuming (11) and (12) are satisfied, (which later will be considered as a constraint), the sign of S_x and S_y can be used to determine in which quadrant γ should reside. The four different possibilities are shown in Fig. 4. For example, if $S_x > 0$ and $S_y < 0$, in order to have a decreasing error it is needed to have $\dot{S}_x < 0$ and $\dot{S}_y > 0$, which is equivalent to $\sin\gamma < 0$ and $\cos\gamma < 0$ or having γ in the 3^{rd} quadrant. Moreover, in order to incorporate the magnitude of

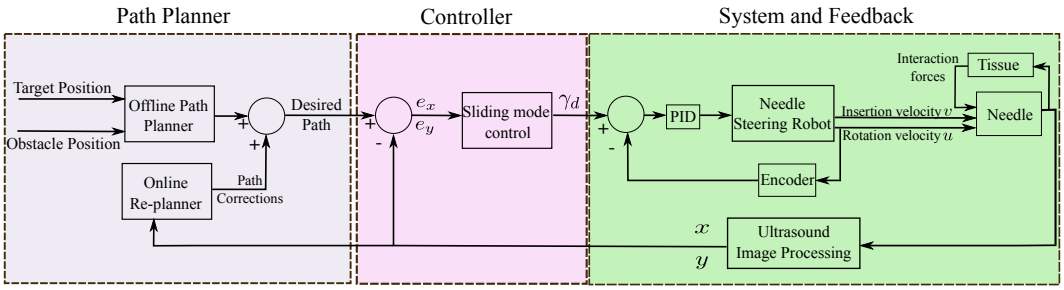

Figure 3: The closed-loop structure consisting of system, controller and path planner.

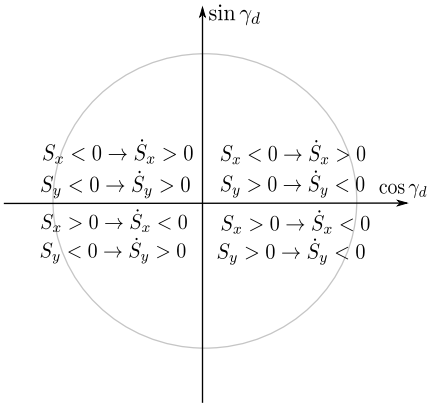

Figure 4: The four possibilities for S_x and S_y and the corresponding quadrant for γ_d.

the sliding surfaces S_x and S_y in compensating the error, the desired angle γ_d is defined as

$$\gamma_d = \text{atan2}(-S_x, S_y) \tag{13}$$

where $\gamma_d \in [-\pi, \pi]$ and the function atan2 is the tangent inverse function, which takes into account the sign of the two inputs to return the appropriate quadrant of the calculated angle. This selected quadrant (or mode) plays the main role in decreasing the error as it ensures that both sliding surfaces S_x and S_y decrease simultaneously.

To ensure that (11) and (12) are satisfied simultaneously, the system parameters can be selected such that these two inequalities are satisfied for the worst case of α and β. Assume $|\alpha| < \alpha^*$ and $|\beta| < \beta^*$ where $\alpha^* > 0$ and $\beta^* > 0$ are the bounds of angles α and β, respectively. The above inequalities can be written as

$$\begin{aligned} &\arcsin\left(\frac{1}{b_x k v}\tan\beta^*\right) < |\gamma_d| < \\ &\arccos\left(\sin\beta^*\tan\alpha^* + \frac{1}{b_y k v}\cos\beta^*\tan\alpha^*\right) \end{aligned} \tag{14}$$

in which α and β are substituted by α^* and β^*, respectively. The values of b_x, b_y and the upper bounds α^* and β^* should be selected such that the arguments of arcsin and arccos are less than 1 and (14) is feasible. According to the target point, the value of α^* and β^* can be determined in the planning level considering that larger values of α^* and β^* correspond to more needle bending leading to a larger reachable workspace.

This condition is also affected by the value of the sliding surface parameters, b_x and b_y, which should be selected in accordance with α^*, β^* and k. According to (4) and (5), in order to have a faster response, it is desired to have smaller values of of b_x and b_y because they determine the convergence time of e_x and e_y as S_x and S_y tend to zero. However, this condition forces α^* and β^* to be small to make (14) feasible. The effect of α^*, β^* and $b_i\,(i = x, y)$ on the desired value γ_d is shown in Fig. 5 for $k = 0.002$ mm^{-1} and $b_x = b_y$. Fig. 5(a) and 5(b) show that small values of α^* and β^* lead to a larger range for γ_d. For example, if $\alpha^* = \beta^* = 0$, (14) simplifies to $0 < |\gamma_d| < \pi/2$, the maximum acceptable region. In this case, the sliding surface parameters can be selected arbitrarily, however, having $\alpha^* = \beta^* = 0$ is equivalent to having no deflection at the needle tip throughout the insertion, which according to the physical nature of the system is not possible. Moreover, increasing α^* and β^* makes the acceptable range for γ_d smaller until no value for γ_d can be found. Fig. 5(c) shows the effect of sliding parameter $b_x = b_y$ for the fixed values of $\alpha^* = \beta^* = 0.2$ rad. As it can be seen, by increasing b, the feasible range for γ_d gets larger, and smaller values of $b_i\,(i = x, y)$ might lead to a non-feasible value for γ_d.

3.2. Adaptive Structure

As stated before, it is desired to have small sliding surface parameters as they determine the con-

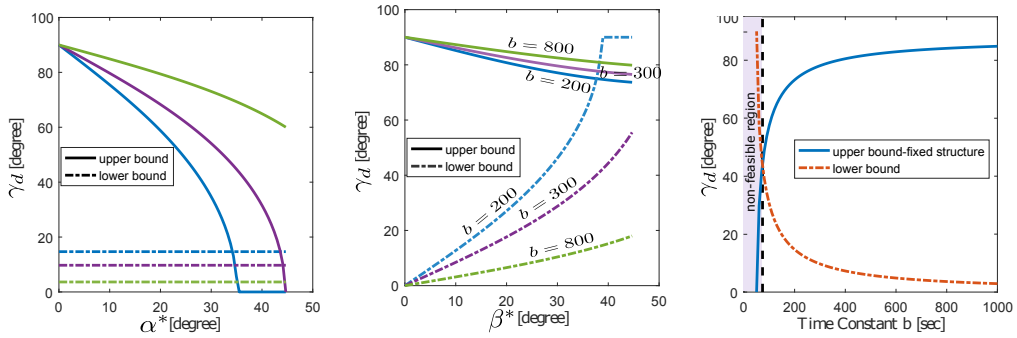

Figure 5: The effect of the design parameters on the feasible range of γ_d for $k = 0.002$ mm$^-$1 and $b_x = b_y = b$. (a) shows the effect of increasing α^* for different values of b and $\beta^* = 0.2$ rad. (b) shows the efect of increasing β^* for different values of b and $\alpha^* = 0.2$ rad. (c) shows the effect of increasing b for $\alpha^* = \beta^* = 0.2$ rad.

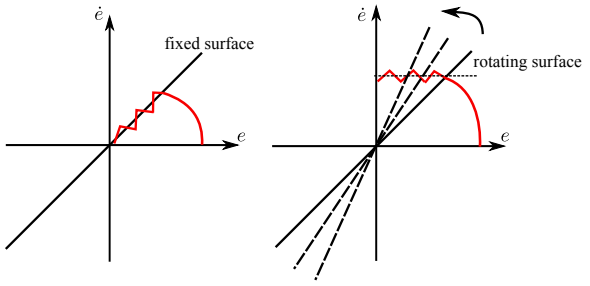

Figure 6: Fixed and adaptive sliding surfaces in the phase plane.

vergence time of the error in both the x and y directions. From (3), it is clear that as the needle is moving forward, there are no equilibrium points for the system and it is not possible to make the time derivative of the system state errors zero. Using the sliding surface in the previous section, the system is pushed toward the constant sliding surface and kept as close as possible to this surface, which moves the errors in the x and y directions and their first derivative toward zero. Since the time derivatives of the system states are changing, it is only possible to focus on the deflection error and not its derivative. This can be done by rotating the sliding surface at a constant rate in such a way that as the needle is inserted, the error signals in the x and y directions approach zero. This is shown in Fig. 6. The sliding surfaces defined by (4) and (5) represent a line in the phase plane whose slope equals $\frac{1}{b_i}$ $(i = x, y)$. By changing b_i, the lines rotate about the origin. As it is shown, by increasing the slope of the line and rotating the sliding surface toward the vertical axis, the error in the phase plane approaches zero. In this case, the sliding surfaces are defined as in (4) and (5) but the parameters b_x and b_y are variable, which leads to

$$\dot{S}_i = b_i \ddot{e}_i + \dot{e}_i \left(\dot{b}_i + 1 \right), \; i = x, y \tag{15}$$

Selecting $\dot{b}_i = -1$ leads to

$$\dot{S}_x = b_x k v \cos\beta \sin\gamma \tag{16}$$

$$\dot{S}_y = -b_y k v \cos\alpha \cos\gamma + b_y k v \sin\beta \sin\alpha \sin\gamma \tag{17}$$

It should be noted that the parameters b_x and b_y should always be positive. This can be guaranteed by knowing the desired insertion depth, D, the constant insertion velocity, v, and choosing the initial value $b_i(0) \geq \frac{D}{v}$. With the proposed fixed and adaptive structures, the rotating sliding surface removes the constraint imposed by (11) and relaxes the constraint imposed by (12) as

$$|\tan\gamma_d| < \frac{1}{\sin\beta^* \tan\alpha^*} \tag{18}$$

in which there is no dependence on the needle path curvature k. This condition is obtained for the worst case representing a conservative performance. The effect of this saturation is shown in Fig. 7 by performing simulations for different values of the upper bound for γ_d and ignoring the stability. The results are shown for $b(0) = 80$, with an insertion velocity of 2 mm/sec, a maximum insertion depth of 140 mm, and the desired path being a straight line. The figure shows that the effects of limiting γ_d is negligible; however, having saturation on γ_d ensures the stability of the system. In the fixed

structure, the value of sliding surface parameters b_i are lower bounded due to the constraints imposed by the stability condition, and for these fixed values, the weight of the error in the sliding surface does not change. In the adaptive structure, as the needle reaches the desired depth, b_i gets smaller and the position error in the sliding surface gets more heavily weighted, leading to smaller errors.

Equations (16) and (17) obtained for the adaptive structure, are simpler than (8) and (9), for which (13) still ensures $\dot{S}_x S_x < 0$ and $\dot{S}_y S_y < 0$. Assuming $\gamma = \gamma_d$ at each time interval, substituting γ_d in (16) gives:

$$\dot{S}_x < -\eta_x S_x, \quad S_x > 0 \tag{19a}$$
$$\dot{S}_x > -\eta_x S_x, \quad S_x < 0 \tag{19b}$$

$$\dot{S}_y < -\eta_y S_y, \quad S_y > 0 \tag{20a}$$
$$\dot{S}_y > -\eta_y S_y, \quad S_y < 0 \tag{20b}$$

with

$$\eta_x = \frac{b_x k v \cos\beta^*}{\sqrt{S_{x0}^2 + S_{y0}^2}} > 0 \tag{21a}$$
$$\eta_y = \frac{b_y k v |\cos\alpha - \cos\alpha^*|}{\sqrt{S_{x0}^2 + S_{y0}^2}} > 0 \tag{21b}$$

where S_{x0} and S_{y0} are the values of S_x and S_y, at the beginning of the time interval, respectively. Multiplying the sides of (19) and (20) by S_x and S_y, respectively, gives $S_x\dot{S}_x < -\eta_x S_x^2$ and $S_y\dot{S}_y < -\eta_y S_y^2$, which show the finite time convergence of the sliding surface during the reaching phase.

3.3. Stability

It should be noted that according to the physical properties of the system, it is not possible for the three angles, representing the orientation, to go unbounded. With its desired value being γ_d, which is bounded, the roll angle will obviously remain bounded. Unbounded β and α would be equivalent to the needle tracking a full circle in the tissue, which according to the curvature of the needle and in the presence of tissue, is not possible. However, In order to use the proposed method, the system states should stay in (2) so that the equations are valid. Since the control law is updated at the beginning of the intervals, assuming $\gamma = \gamma_d$ and taking its time derivative gives

$$\dot{\gamma} = -\frac{\dot{S}_x S_y - \dot{S}_y S_x}{S_x^2 + S_y^2} = -\cos\gamma \tan\beta \tag{22}$$

from which

$$\tan\beta = \frac{1}{\cos\gamma}\frac{\dot{S}_x S_y - \dot{S}_y S_x}{S_x^2 + S_y^2} \tag{23}$$

Note that $\cos\gamma \neq 0$ as γ is selected according to (18). Consider the following Lyapunov function:

$$V = \frac{1}{2}\left(\tan^2\beta + M\left(S_x^2 + S_y^2\right)\right) \tag{24}$$

Here, M is a large positive constant. Taking time derivative of (24) and substituting from (23) and using $\tan\gamma = \frac{S_x}{S_y} sgn(S_x S_y)$ gives

$$\dot{V} = S_x\dot{S}_x\left(M + kv\frac{sgn(S_xS_y)(1+\tan^2\beta)}{S_x^2+S_y^2}\right) + S_y\dot{S}_y\left(M - kv\frac{sgn(S_xS_y)(1+\tan^2\beta)S_x^2}{(S_x^2+S_y^2)S_y^2}\right) \tag{25}$$

Since $S_x\dot{S}_x < 0$ and $S_y\dot{S}_y < 0$, choosing $M > max(kv\frac{(1+\tan^2\beta^*)}{S_x^2+S_y^2}), kv\frac{(1+\tan^2\beta^*)S_x^2}{(S_x^2+S_y^2)S_y^2})$, the above equation ensures that $\dot{V} \leq 0$, which is equivalent to V being decreasing during the reaching phase, in which $S_x \neq 0$ and $S_y \neq 0$. During the sliding (i.e. chattering) phase, if $S_x = 0$ then $\gamma_d = 0$ and still the above inequality holds. If $S_y = 0$, γ_d should be saturated by the constraint (18), for which $\dot{\gamma} \neq 0$ and S_y moves away from zero. This shows that V remains bounded or $\beta \neq \pm\pi/2$.

It should be noted that β^* is selected properly according to the application and the needle/tissue specifications as follow. From the system equations (3), $|\dot{\beta}| \leq kv$. Starting from zero initial condition (which is true as the needle is unbent at the beginning), the maximum value of β can be found by taking integral of this inequality. Since the needle length, L, is bounded and the variations of the needle length inside the tissue is $\dot{\ell} = v$ the maximum value of β can be found as $\beta < kL$. Using this maximum value, β^* can be selected accordingly. In practice, since the needle path curvature is small and the needle length is limited, $|\beta|$ will also remain bounded and less than β^*. Similar discussion can be made for the angle $|\alpha|$.

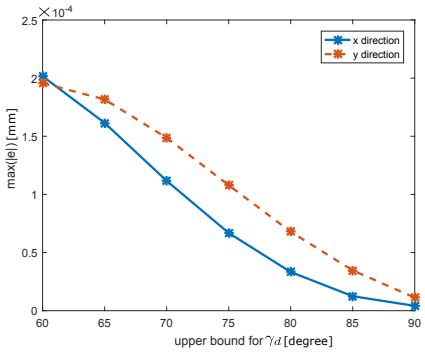

Figure 7: The effect of upper bound on γ_d on performance in simulations for moving the needle on a straight line.

3.4. Simulations

In this section simulations are presented to study the effectiveness of the proposed method and to compare it with other methods proposed in the literature. Here, the proposed method is compared with methods based on continuous rotations [12, 18]. In practical applications, it is desired to limit the number of needle rotations since too many rotations may cause tissue damage and trauma by cutting the tissue and by heating produced by needle/tissue friction. This issue has been previously studied in the literature [29, 30]. The tissue trauma can be measured as the heat and energy transferred to the tissue caused by needle rotations. The measure for tissue trauma is defined as

$$\text{Trauma} = \int_0^t u^2 dt \tag{26}$$

where t is the insertion time and u is the rotational velocity. The simulations are performed for the adaptive structure proposed in the previous section with an insertion velocity of 2 mm/sec and an insertion depth of 140 mm. The constant rotational velocity for the comparison is selected as 2π rad/sec and the desired performance is to move the needle on a straight line. As a needle rotates with constant velocity, it moves on a helical path whose radius depends on the rotational velocity, faster rotations leading to smaller errors. However, this behavior gives rise to the drilling effect, which causes tissue trauma. In our proposed method, the needle is only rotated when necessary, which is equivalent to making small adjustments to reduce the error in both the x and y directions. The results depicted in Fig.8 show that the proposed method yields a maximum position error of 0.08 mm, which is still negligible, but results in reduced trauma on tissue.

4. Steering in the presence of obstacles

4.1. Path Planner

In the presence of anatomical obstacles, the needle should be guided on a pre-planned path. This path should be found as a feasible trajectory that minimizes the targeting error and avoids any obstacles. In this case, the steering problem turns into a trajectory tracking problem, which is explained in the next section. The control method proposed in the previous section is a general controller that does not depend on any specific planning method as only the position error and its time derivative are involved in the control algorithm. The feasible path can be found using offline path planning methods. However, the targeting accuracy can be improved by doing online re-plannings to compensate for any disturbances caused by tissue inhomogeneity. This online re-planning can be updated at a slower rate with respect to the control loop to ensure that there will be a feasible path from the current position to the target while maneuvering around the obstacles.

Here, an offline path planner is used to find a desired path that reaches the target point and avoids collisions with anatomical obstacles. The location of the target point and the obstacles are determined by pre-operation scans which are fed to the planner which uses the kinematic 3D unicycle equations (3). In this planning method, the insertion depth is divided into n points at which needle rotations should occur. The values of the needle roll angle at these n intervals are the output of the planner. Having the closed form response [19], Algorithm 1 can be used to find the rotation values at n samples. In this algorithm, the function `costfunction` calculates the tip deflection at each sample n and also at the obstacle to minimize the tip deflection error at the target and maximize the distance from the obstacle. However, the proposed control method is not limited to this planner and any other offline or online path planning methods can be used to produce the desired trajectory or make corrections to find a feasible path from current needle's position to the target.

4.2. Tracking Method

The desired path generated by the planner is the reference input to the control loop that should be

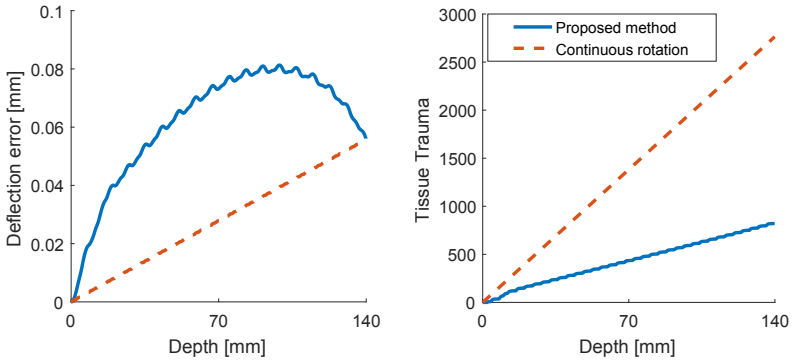

Figure 8: Simulation results comparing the deflection and tissue trauma for different methods with the desired trajectory of a straight line. (a): Norm of needle tip deflection. (b): Tissue trauma

Algorithm 1: Path Planner

```
Initialize : T_0
Select T randomly
Cost_0 = costfunction(T_0)
while i < Max_iteration do
    Cost = costfunction(T)
    if Cost < Cost_0 then
        T_0 ← T
        Cost_0 ← Cost
    end
    else if
    prob(Cost, Cost_0, T_0, T) > random() then
        T_0 ← T
        Cost_0 ← Cost
    end
    update(T)
    i = i + 1
end
```

followed by the needle tip. The sliding mode controller is then responsible for calculating the angle γ_d to make this tracking happen. The difference between a desired trajectory and a straight line is that the time derivatives of the desired trajectory are not necessarily zero. However, in the constraints derived in section 3, it is assumed $\dot{x}_d = \ddot{x}_d = \dot{y}_d = \ddot{y}_d = 0$. In order to apply the same conditions and control strategy to trajectory tracking, it is possible to discretize the desired path by sampling and holding to break the tracking problem into several small regulation problems. In this method, the desired trajectory turns into a set of successive small steps, each of which should be reached by the needle during the discretization sample time. In order to have small errors at the end of each step, a sawtooth wave is applied to the sliding surface parameters b_x and b_y by resetting them at each discretization step to their initial values such that they remain positive all the time. This discretization is the only modification made for the tracking problem and can be performed at the planner/re-planner level.

5. Experiments

To verify the accuracy of the proposed controller, the experimental setup shown in Fig. 9 is used. The system consists of a carriage actuated by a DC motor through a belt and pulley mechanism which performs the translational motion of the needle. Another DC motor is assembled on the translational stage to which the needle base is attached, and performs the needle axial rotations. This motor is equipped with an encoder and its position is controlled using a PID controller. In our experiments highly flexible notched needles proposed in [31] with experimentally identified mean deflection radius of curvature of 400 mm are used. The phantom tissue used in these experiments is plastisol, made of 80% liquid plastic and 20% plastic softener (M-F Manufacturing Co., Fort Worth, TX, USA) with an estimated Young's modulus of elasticity of 35 kPa. To track needle tip, 2D transverse ultrasound images are used (SonixTouch, Ultrasonix, BC, Canada), which provide information about the needle position. In clinical manual insertions, the surgeon uses the ultrasound images visually to track the needle. Here this visual feedback is combined with image processing and Kalman filtering technique to calculate the needle tip deflection from partial observations of the needle [32]. Since the

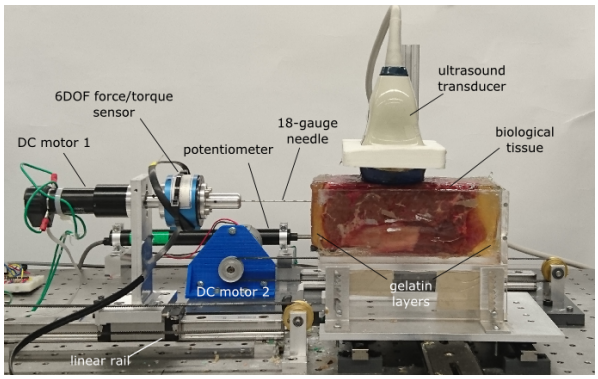

Figure 9: Experimental setup used to perform needle insertion. The setup provides translational and rotational motion of the needle. An ultrasound machine (SonixTouch, Ultrasonix, BC, Canada) is used to track the needle tip position. A 6DOF force/torque sensor is attached to the needle base which is not used in these experiments. The phnatom tissue used in these experiments is plastisol.

ultrasound images are the only source providing us with the needle tip position, this information should be accepted as the true measurement value. However, in order to find the tip position, the needle tip should be visible in the images. Issues about the required image quality and different artifacts affecting the needle position measurement are discussed in [32], which is out of scope of this work. Here, the information obtained from ultrasound images is considered as the true value of the needle tip deflection, which provides numerical measurements to be used by the controller. The needle tip deflection is fed back to the controller and is updated every 0.05 sec. The ultrasound probe is attached to a translational platform to track the needle tip.

The position signal is then filtered to reduce noise and the velocity is found by taking the time derivative of the position signal. Since the needle tip deflection changes are much slower than the noise imposed on the signals, the effects of the filter on the system dynamics can be neglected.

The insertions are performed for a constant insertion velocity of $v = 2$ mm/sec. The settling time of the needle axial rotation with the PID controller is about 0.2 sec, which is considered in the update time of the desired value γ_d. The upper bounds α^* and β^* are selected as 0.15 rad. The experiments are performed in two different scenarios, in each of which eight trials were conducted.

In the first scenario, the needle is inserted to the desired depth of 140 mm and aimed to move on a straight line as in a conventional brachytherapy procedure, i.e., $x_d = y_d = 0$. The initial value $b(0)$ is selected to be 80. The results indicate a mean absolute error of 0.54 ± 0.37 and 0.23 ± 0.2 mm and a maximum targeting error of 1.0 and 0.81 mm for the x and y directions, respectively, as summarized in Table 1. The needle tip error for different trials as well as the needle tip track for one of the trials are shown in Fig. 10 and Fig. 11. In the second scenario, the needle is inserted to the target point at a depth of 140 mm and is steered to avoid an obstacle at the depth of a 80 mm to simulate pubic arc interference (PAI) [33], which is common in patients with a large prostate. PAI obstructs the needle path to the anterior prostate, resulting in poor seed placement and dose reduction [34]. According to [35], the average prostate size for men between the ages of 40 and 50 is 44 mm in width, 31 mm in height and 37 mm in length. To simulate a severe PAI, a 10 mm interference between pubic arch and prostate is considered and modeled as an obstacle with radius of 2 mm. Using these criteria, a desired path is generated using the offline algorithm introduced in section 4.1 for $n = 5$.

Here, the path is the reference to the closed-loop system and the controller keeps the needle on the desired path.

The path generated by the planner is then discretized by a sample time of 1 sec. The initial values of the sliding surface parameters b_i are selected as 3, which are reset to their initial values every 1 second. From Table 1, the mean absolute error of 0.48 ± 0.55 and 0.51 ± 0.61 mm is obtained for the x and y directions, respectively. The maximum targeting error is 1.14 mm for the x direction and 1.03 mm for the y direction. The needle tip error for eight trials and tip position for one of the trials are shown in Fig. 10 and Fig.11, respectively. The experimental results show a maximum position error of 1.14 mm.

6. Concluding Remarks

In this paper, a non-model-based control structure for steering beveled-tip needles in soft tissue is presented. In this control scheme, two sliding surfaces are defined to account for the needle tip deflection error in the x and y directions as the needle is inserted to reach the desired depth. The controller's output is the needle's roll angle, which is calculated using the sliding surfaces. The proposed method only uses the information about the needle tip position obtained from the ultrasound

Table 1: Summary of the experimental results

Desired Position	Results- x direction: Mean Absolute Error [mm]	Standard deviation (σ)	RMSE [mm]	Max Targeting Error [mm]	Results-y direction: Mean Absolute Error [mm]	σ	RMSE [mm]	Max Targeting Error [mm]
1^{st} scenario	0.54	0.37	7.3×10^{-5}	1.0	0.23	0.20	6.1×10^{-5}	0.81
2^{nd} scenario	0.48	0.55	1.5×10^{-4}	1.14	0.51	0.61	6.6×10^{-5}	1.03

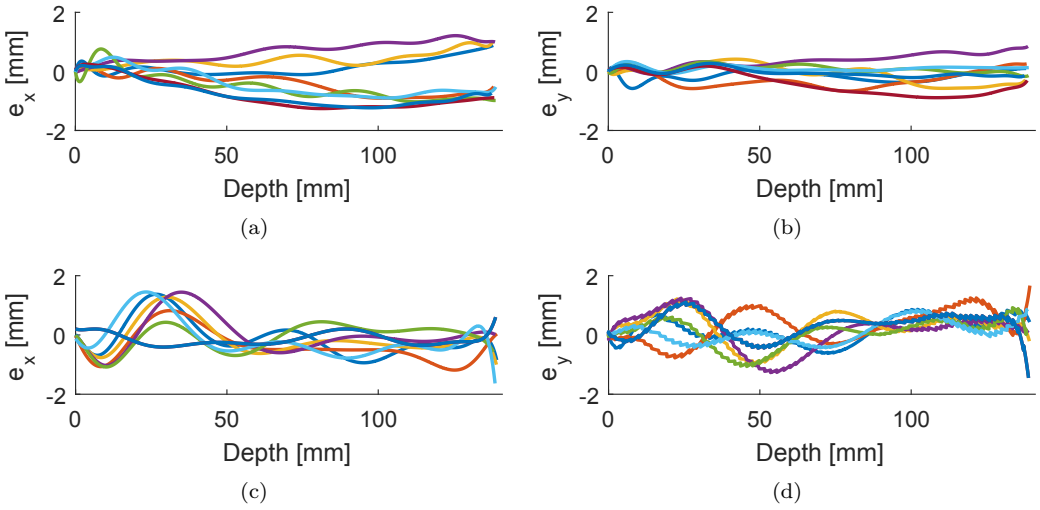

Figure 10: Needle tip error for needle insertion in plastisol tissue. (a),(b): show the needle tip error for 8 trials in the x and y directions for moving on a straight line ($x_d = 0$ mm, $y_d = 0$ mm). (c),(d): show the needle tip error for 8 trials in the x and y directions for moving on a desired trajectory.

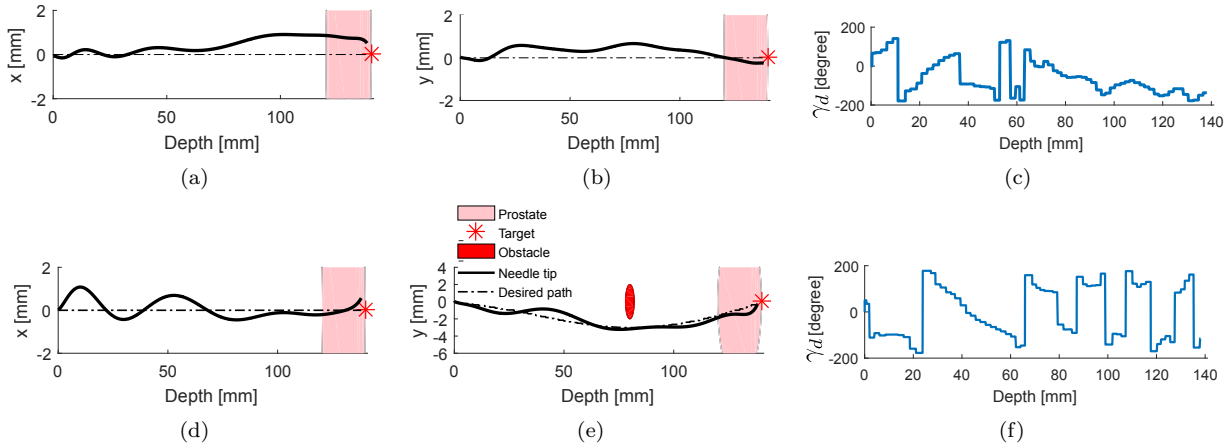

Figure 11: Representative results for needle insertion in plastisol tissue for two scenarios: (a),(b),(c): moving on a straight line; (d),(e),(f): moving on a desired trajectory. (a) and (b) show the needle tip position in the x and y directions and (c) is the desired needle roll angle obtained from the sliding mode controller. (d) and (e) show the needle tip position in the x and y directions and (f) is the desired needle roll angle obtained from the sliding mode controller.

images and no information about the needle tip orientation is involved in finding the control action. The convergence of the deflection error is shown using the 3D unicycle equations. The constraints imposed by this convergence analysis are relaxed using a adaptive-structure controller and rotating the sliding surfaces. To evaluate the proposed controller, experiments are performed on phantom tissue for an environment with and without an obstacle. To go around the obstacle, a path planner is used which is based on optimization methods and finds a feasible path as the reference input to the control loop. From the experiments, the mean absolute and maximum error are 0.5 mm and 1.14 mm, respectively, which are comparable with the results in the literature. In this work, the target locations are considered to be stationary and the experiments are performed on phantom tissue. Further developments will include the presence of moving targets and needle insertions in biological tissue.

7. Acknowledgments

This work was supported by the Natural Sciences and Engineering Research Council (NSERC) of Canada under grant CHRP 446520, the Canadian Institutes of Health Research (CIHR) under grant CPG 127768 and the Alberta Innovates - Health Solutions (AIHS) under grant CRIO 201201232.

References

[1] C. Rossa, M. Tavakoli, Issues in closed-loop needle steering, Control Engineering Practice 62 (2017) 55–69.

[2] R. Alterovitz, M. Branicky, K. Goldberg, Constant-curvature motion planning under uncertainty with applications in image-guided medical needle steering, in: Algorithmic Foundation of Robotics VII, Springer, 2008, pp. 319–334.

[3] N. Abolhassani, R. V. Patel, F. Ayazi, Minimization of needle deflection in robot-assisted percutaneous therapy, The international journal of medical Robotics and computer assisted surgery 3 (2) (2007) 140–148.

[4] W. Park, J. S. Kim, Y. Zhou, N. J. Cowan, A. M. Okamura, G. S. Chirikjian, Diffusion-based motion planning for a nonholonomic flexible needle model, in: Proceedings of the 2005 IEEE International Conference on Robotics and Automation, 2005. ICRA 2005., IEEE, 2005, pp. 4600–4605.

[5] S. P. DiMaio, S. Salcudean, Needle steering and motion planning in soft tissues, IEEE Transactions on Biomedical Engineering 52 (6) (2005) 965–974.

[6] R. Alterovitz, K. Goldberg, A. Okamura, Planning for steerable bevel-tip needle insertion through 2D soft tissue with obstacles, in: Proceedings of the 2005 IEEE International Conference on Robotics and Automation, 2005. ICRA 2005., IEEE, 2005, pp. 1640–1645.

[7] J. Xu, V. Duindam, R. Alterovitz, K. Goldberg, Motion planning for steerable needles in 3D environments with obstacles using rapidly-exploring random trees and backchaining, in: IEEE International Conference on Automation Science and Engineering, 2008. CASE 2008., IEEE, 2008, pp. 41–46.

[8] V. Duindam, R. Alterovitz, S. Sastry, K. Goldberg, Screw-based motion planning for bevel-tip flexible needles in 3D environments with obstacles, in: IEEE International Conference on Robotics and Automation, 2008. ICRA 2008., IEEE, 2008, pp. 2483–2488.

[9] K. B. Reed, V. Kallem, R. Alterovitz, K. Goldbergxz, A. M. Okamura, N. J. Cowan, Integrated planning and image-guided control for planar needle steering, in: 2nd IEEE RAS & EMBS International Conference on Biomedical Robotics and Biomechatronics, 2008. BioRob 2008., IEEE, 2008, pp. 819–824.

[10] G. J. Vrooijink, M. Abayazid, S. Patil, R. Alterovitz, S. Misra, Needle path planning and steering in a three-dimensional non-static environment using two-dimensional ultrasound images, The International journal of robotics research (2014) 0278364914526627.

[11] S. Patil, J. Burgner, R. J. Webster, R. Alterovitz, Needle steering in 3-d via rapid replanning, IEEE Transactions on Robotics 30 (4) (2014) 853–864.

[12] D. S. Minhas, J. A. Engh, M. M. Fenske, C. N. Riviere, Modeling of needle steering via duty-cycled spinning, in: Engineering in Medicine and Biology Society, 2007. EMBS 2007. 29th Annual International Conference of the IEEE, IEEE, 2007, pp. 2756–2759.

[13] A. Haddadi, O. Goksel, S. E. Salcudean, K. Hashtrudi-Zaad, On the controllability of dynamic model-based needle insertion in soft tissue, in: IEEE International Conference of the Engineering in Medicine and Biology, IEEE, 2010, pp. 2287–2291.

[14] M. Khadem, C. Rossa, N. Usmani, R. S. Sloboda, M. Tavakoli, Semi-automated needle steering in biological tissue using an ultrasound-based deflection predictor, Annals of Biomedical Engineering.

[15] M. Khadem, C. Rossa, N. Usmani, R. S. Sloboda, M. Tavakoli, A two-body rigid/flexible model of needle steering dynamics in soft tissue, IEEE/ASME Transactions on Mechatronics 21 (5) (2016) 2352–2364. doi:10.1109/TMECH.2016.2549505.

[16] M. Khadem, C. Rossa, R. Sloboda, *et al.*, Ultrasound-guided model predictive control of needle steering in biological tissue, Journal of Medical Robotics Research 01 (01) (2016) 1640007.

[17] M. Abayazid, G. J. Vrooijink, S. Patil, R. Alterovitz, S. Misra, Experimental evaluation of ultrasound-guided 3D needle steering in biological tissue, International journal of computer assisted radiology and surgery 9 (6) (2014) 931–939.

[18] D. C. Rucker, J. Das, H. B. Gilbert, P. J. Swaney, M. I. Miga, N. Sarkar, R. J. Webster, Sliding mode control of steerable needles, IEEE Transactions on Robotics 29 (5) (2013) 1289–1299.

[19] R. J. Webster, J. S. Kim, N. J. Cowan, G. S. Chirikjian, A. M. Okamura, Nonholonomic modeling of needle steering, The International Journal of Robotics Research 25 (5-6) (2006) 509–525.

[20] V. Kallem, N. J. Cowan, Image guidance of flexible tip-steerable needles, IEEE Transactions on Robotics 25 (1) (2009) 191–196.

[21] B. Fallahi, C. Rossa, R. Sloboda, *et al.*, Partial esti-

mation of needle tip orientation in generalized coordinates in ultrasound image-guided needle insertion, in: IEEE International Conference on Advanced Intelligent Mechatronics (AIM), Banff, Canada, 2016, pp. 1186–1191.

[22] B. Fallahi, C. Rossa, R. S. Sloboda, N. Usmani, M. Tavakoli, Sliding-based switching control for image-guided needle steering in soft tissue, IEEE Robotics and Automation Letters 1 (2) (2016) 860–867.

[23] S. J. Dodds, et al., Feedback control, London: Springer (2015) 5.

[24] S.-B. Choi, C.-C. Cheong, D.-W. Park, Moving switching surfaces for robust control of second-order variable structure systems, International Journal of Control 58 (1) (1993) 229–245.

[25] H. Komurcugil, Rotating-sliding-line-based sliding-mode control for single-phase ups inverters, IEEE Transactions on Industrial Electronics 59 (10) (2012) 3719–3726.

[26] H. Liang, K. T. Chong, T. S. No, S.-Y. Yi, Vehicle longitudinal brake control using variable parameter sliding control, Control Engineering Practice 11 (4) (2003) 403–411.

[27] F. Li, H.-L. Xie, Sliding mode variable structure control for visual servoing system, International Journal of Automation and Computing 7 (3) (2010) 317–323.

[28] C. Rossa, N. Usmani, R. Sloboda, M. Tavakoli, A hand-held assistant for semi-automated percutaneous needle steering, IEEE Transactions on Biomedical Engineering.

[29] T. Podder, D. Clark, D. Fuller, J. Sherman, W. Ng, L. Liao, D. Rubens, J. Strang, E. Messing, Y. Zhang, et al., Effects of velocity modulation during surgical needle insertion, in: IEEE-EMBS 2005. 27th Annual International Conference of the Engineering in Medicine and Biology Society, 2005., IEEE, 2005, pp. 5766–5770.

[30] P. J. Swaney, J. Burgner, H. B. Gilbert, R. J. Webster, A flexure-based steerable needle: high curvature with reduced tissue damage, IEEE Transactions on Biomedical Engineering 60 (4) (2013) 906–909.

[31] M. Khadem, C. Rossa, R. Sloboda, *et al.*, Introducing notched flexible needles with increased deflection curvature in soft tissue, in: IEEE International Conference on Advanced Intelligent Mechatronics (AIM), Banff, Canada, 2016, pp. 1186–1191.

[32] M. Waine, C. Rossa, R. Sloboda, N. Usmani, M. Tavakoli, Three-dimensional needle shape estimation in trus-guided prostate brachytherapy using 2-d ultrasound images, IEEE journal of biomedical and health informatics 20 (6) (2016) 1621–1631.

[33] K. Wallner, W. Ellis, K. Russell, W. Cavanagh, J. Blasko, Use of trus to predict pubic arch interference of prostate brachytherapy, International Journal of Radiation Oncology Biology Physics 43 (3) (1999) 583–585.

[34] J. Fukada, N. Shigematsu, J. Nakashima, T. Ohashi, O. Kawaguchi, M. Oya, Predicting pubic arch interference in prostate brachytherapy on transrectal ultrasonography-computed tomography fusion images, Journal of radiation research (2012) 753–759.

[35] S.-J. Zhang, H.-N. Qian, Y. Zhao, K. Sun, H.-Q. Wang, G.-Q. Liang, F.-H. Li, Z. Li, Relationship between age and prostate size, Asian J Androl 15 (1) (2013) 116–120.